Applied Catalysis B: Environmental 184 (2016) 132–141

Contents lists available at ScienceDirect

Applied Catalysis B: Environmental

journal homepage: www.elsevier.com/locate/apcatb

Mesoporous sulfur-modified iron oxide as an effective Fenton-like catalyst for degradation of bisphenol A

Jiangkun Du [a], Jianguo Bao [a,*], Xiaoyan Fu [a], Chenghang Lu [a], Sang Hoon Kim [b,**]

[a] School of Environmental Studies, China University of Geosciences, Wuhan 430074, PR China
[b] Center for Materials Architecturing, Korea Institute of Science and Technology, Seoul 136-791, Republic of Korea

ARTICLE INFO

Article history:
Received 9 September 2015
Received in revised form
13 November 2015
Accepted 15 November 2015
Available online 18 November 2015

Keywords:
Mesoporous sulfur-modified iron oxide
Bisphenol A
Fenton-like oxidation

ABSTRACT

A mesoporous sulfur-modified iron oxide (MS-Fe) was prepared as a heterogeneous H_2O_2 catalyst for degradation of BPA. The physico-chemical properties of MS-Fe and bare M-Fe were characterized by BET surface area measurement, SEM, XRD, FTIR and XPS. Both M-Fe and MS-Fe composites appeared as cubic microparticles with abundant pores and cracks as well as large surface area. As depicted by XRD, EDX and XPS, M-Fe is mainly consisted of hematite while MS-Fe is a kind of S-doped iron oxide with about 5–6% of sulfur element in terms of atomic ratio. In contrast to the poor catalytic activity of bare M-Fe, the MS-Fe composites showed greatly improved efficiencies for H_2O_2 activation for BPA degradation. The high catalytic activity of this new Fenton-like catalyst can be obtained at different initial pH in range of 3.0–9.0. The time evolution of degradation of BPA followed pseudo-first-order kinetics, and the first-order rate constants showed a linear relationship with parameters of initial pH, catalyst dosage and concentration of BPA. However, the H_2O_2 dosage showed a dual effect on BPA degradation because excessive H_2O_2 addition lead to scavenging of hydroxyl radicals (•OH). The investigation of working mechanisms of MS-Fe suggested a synergistic effect of homogeneous and heterogeneous degradation reaction, wherein a strong acidic environment, abundant surface-bonded hydroxyl group and electron-mediating effect of sulfur all contributed to fast activation of H_2O_2. Overall, this new material overcomes the limitation of narrow working pH range and shows a fast oxidation of BPA with a low H_2O_2 and catalyst dosage, would have a good potential for environmental application.

1. Introduction

To satisfy rapid development of modern agriculture, chemical industry and human activities, an increasing number of man-made chemicals have been produced. Since most of these industry-derived chemicals never existed in natural environment before, they are hardly biodegradable and many of them exhibited considerable toxicity to microorganisms [1]. A growing number of evidence show that substantial amount of synthetic chemicals have been released into the environment, causing serious environmental concerns on the safety of ecosystem and human health [2,3]. Therefore, proper treatments should be carried out to remove these undesired contaminants from wastewater, groundwater and even drinking water. Advanced oxidation processes (AOPs) is an efficient and extensively used treatment technology for water purification. Fenton process using hydrogen peroxide (H_2O_2) as oxidant precursor is one of the strongest AOPs, and recognized to be environmentally benign since only H_2O and O_2 are produced after reaction [4]. The decomposition of H_2O_2 would generate powerful hydroxyl radical (•OH) which possess a high standard oxidation potential [E^0(•OH/H_2O) = +2.8 V_{NHE}] and is able to non-selectively degrade and mineralize most organic pollutants under ambient conditions [5,6]. Therefore, Fenton processes are increasingly attractive for removing non-biodegradable and recalcitrant organic compounds in aquatic system.

In conventional Fenton processes, iron salts specially ferrous salts were usually used as catalyst to activate H_2O_2. Although these homogeneous Fenton processes are simple and effective, they face problems of low operation pH range (normally 3–4) and difficulty of catalyst separation from the effluent leading to generation of ferric hydroxide sludge [5,7]. To reduce these negative effects, many heterogeneous Fenton-like catalysts have been developed to provide an alternative solution for iron precipitation, contributing to a higher pollutant mineralization efficiency above pH 4 [8,9]. Iron-bearing materials, such as zero-valent iron, pyrite, iron oxides,

* Corresponding author. Fax: +86 27 87436235.
** Corresponding author. Fax: +82 2 9 585447.
E-mail addresses: bjianguo@cug.edu.cn (J. Bao), kim_sh@kist.re.kr (S.H. Kim).

http://dx.doi.org/10.1016/j.apcatb.2015.11.015
0926-3373/

have been densely studied for Fenton-like reactions. Iron oxides have attracted more attention because they are abundant, cheap, chemically and thermally stable, and easy to synthesize and separate [7,10]. Moreover, the leaching of iron ions from iron oxides is much lower compared to zero-valent iron, thus they can reduce sludge formation and facilitate post-treatment. Nevertheless, there are several drawbacks of applying iron oxides to Fenton-like reactions. For instance, Fe(III) is the main iron species of iron oxides but the reaction rate of Fe(III)/H_2O_2 is much slower than that of Fe(II)/H_2O_2 [7,11,12]. In addition, limited mass transfer of heterogeneous system would result in low reactivity of H_2O_2 decomposition. Furthermore, high concentration of H_2O_2 and iron dosage are required to achieve satisfied reaction efficiencies [13]. Hence the development of highly efficient iron-based Fenton catalyst has become indispensible. Therein, materials with porous structures have attracted increasing research interests because of their high surface area and pore volume [8,14]. Ursachi et al. reported the preparation of α-Fe_2O_3 stabilized inside the pore system of mesoporous silica MCM-41 [15]. The α-Fe_2O_3/MCM-41 showed effective performance on catalyzing H_2O_2 for methylene blue degradation at pH 3. Coelho et al. compared the effect of iron precursor on the Fenton-like activity of mesoporous silica imbedded Fe_2O_3 [16]. Their results showed that Fe_2O_3/mesoporous silica prepared using ferric precursor was more active than that using ferrous precursor, because the Fe^{3+} oxide nanoparticles were better dispersed on the silica support, resulting in more active sites for H_2O_2 activation. Expect for immobilization on porous hard template, porous iron oxides could also be synthesized by oxalate precipitation followed by calcinations [17]. The decomposition of oxalate into CO_2 under high temperature (above 200 °C) would result in the generation of densely distributed micropores. The preparation method could avoid detachment of iron oxides and low catalyst immobilization efficiency due to the impregnation of iron ions on the meso/micro-porous supports.

Besides enlarging the surface area, iron oxides can also be improved via surface or structural modification, such as chelating EDTA or organic surfactants, substitution of iron with other transition metals, to promote their reactivity [18,19]. However, the introduction of EDTA or heavy metals as catalyst component should be carefully considered with respect to their risk of biotoxicity. Very recently, materials doped with element sulfur have shown improved catalytic activity compared with non-doped ones [20]. Guo et al. for the first time prepared S-doped α-Fe_2O_3 via hydrothermal precipitation followed by high temperature calcination treatment [21]. This α-Fe_2O_3/S composite showed good photo-Fenton reactivity under UV or visible light irradiation in the presence of H_2O_2. Pu et al. synthesized Fe/S doped granular activated carbon which showed an enhanced reactivity for persulfate activation [22]. Toda et al. used sulfurized limonite, which was obtained from desulfurization of biogases, as Fenton-like catalyst for decomposition of [9]. As a result, sulfur doping has shown potentials for catalytic activity improvement. So far, however, sulfur doping is still far less studied for modification of iron oxides than other dopants.

In this study, we present a novel mesoporous sulfur-modified iron oxide (MS-Fe) via a simple co-precipitation followed by moderate calcinations. We will show that this sulfur-modified iron oxide with abundant porous channels has a very high reactivity for H_2O_2 activation for degradation of bisphenol A (2,2-bis(4-hydroxyphenyl) propane, BPA) in ambient conditions. BPA is a synthetic chemical and popularly used as intermediate for production of plastics and epoxy resins. Since BPA is an endocrine disrupter which could cause serious ecology deterioration, considerable scientific interests have been generated for its destruction. The objectives of this work included (i) evaluation of the effect of sulfur incorporation on the catalyst reactivity; (ii) investigation of the degradation route of BPA; (iii) understanding of the catalytic behavior of the prepared catalyst. To the best of our knowledge, this is the first ever report on this kind of porous sulfur-modified iron oxides and its application in the Fenton-like oxidation of organic pollutants.

2. Materials and experimental procedure

2.1. Chemicals and reagents

The synthetic BPA, *p*-hydroxybenzoic acid (*p*-HBA), benzoic acid (BA), trifluoroacetic acid used in the study were of analytical grade and supplied by Aladdin. Sodium hydroxide (NaOH, AR, ≥99%), hydrogen peroxide (H_2O_2, ≥30%), ferrous sulfate ($FeSO_4·7H_2O$, AR, 99%), sodium thiosulfate ($Na_2S_2O_3·5H_2O$, AR, 99%), oxalate ($C_2H_2O_4·2H_2O$, AR, 99%) and titanium sulfate ($TiSO_4$, AR, 99%) were purchased from Sinopharm Chemical Reagent Co., Ltd., Methanol, ethanol, *tert*-butyl alcohol were obtained from Fisher and supplied as HPLC grade. All solutions were prepared using deionized water with a resistivity of 18.2 mΩ cm.

2.2. Preparation of the MS-Fe catalyst

The MS-Fe composite was synthesized by a template-free method using oxalate as ferrous precipitant. In a typical procedure, 0.02 mol of $C_2H_2O_4·2H_2O$ was dissolved in 50 mL deionized water with magnetic stirring and the solution temperature was raised to 50 °C. Meanwhile, 0.02 mol of $FeSO_4·7H_2O$ and 0.01 mol of $Na_2S_2O_3·5H_2O$ was dissolved and mixed together in 50 mL deionized water at room temperature. Then, under vigorous magnetic stirring the ferrous solution was added dropwise to the above oxalate solution without pH adjustment. After yellow precipitate formed, the resultant solution was transferred to an ice bath to decrease temperature. Then, the suspension was vacuum-filtered, repeatedly washed with deionized water to remove impurities, and then dried at 70 °C in an ambient dry oven (labeled as S/Fe-oxalate and Fe-oxalate assigning to sulfur-modified and non sulfur-modified composites, respectively). Subsequently, the prepared yellow powder was subjected to calcination in air at 300 °C for 1 h with a heating rate of 4 °C min^{-1}. Finally, the obtained products were collected without further grind and labeled as MS-Fe. For preparation of bare mesoporous iron oxide without sulfur-modification, no sodium thiosulfate was added and the resulting product was labeled as M-Fe. Non-porous sulfur-modified iron oxide (labeled as S-Fe) was synthesized via hydroprecipitation with NaOH instead of oxalate (detailed processes are described in Supplementary information (SI) Text S1).

2.3. Characterization of the composite catalyst

The morphology of the as-prepared iron oxide was investigated using field emission scanning electron microscope (FESEM, Quanta 450 FEG, FEI, USA) combined with an energy dispersive X-ray spectroscopy (EDX) for element mapping and transmission electron microscopy (TEM, CM12/STEM, Philips, the Netherlands). X-ray diffraction (XRD, X'Pert PRO, PANalytical B.V., the Netherlands) patterns were reported to determine the mineralogical identity and structures. The chemical state of surface elements was measured by X-ray photoeletron spectroscopy (XPS, VG Multilab 2000, Thermo Electron) using monochromatic 100 eV Al-Kα radiation. The high resolution XPS spectra of the C1s, O1s, Fe2p and S2p were obtained at a pass energy of 25 eV. The spectra were fitted with Gaussian–Lorentzian component to determine the different oxidation states. Fourier transform infrared spectra (FTIR) were measured using a Thermo Fisher Nicolet-6700 spectrometer. The samples were evenly grinded and pressed into tablets

with KBr for the measurement. The BET surface area was measured by N_2 adsorption isotherms at 77 K using a automated surface area and pore size analyzer (ASAP 2020, Micromeritics, USA). Pore volume and pore size distribution plots were obtained by Barrett–Joyner–Halenda (BJH) method using the cylindrical pore model.

2.4. Catalytic degradation experiments

The degradation kinetics, influence of initial pH, catalyst dosage and the concentration of H_2O_2 on BPA degradation performance were determined by batch experiments. All batch experiments were carried out in 250 mL vessels containing 100 mL reaction solution with predetermined concentration of BPA. The solution pH was not adjusted except for testing the effect of initial pH on degradation behavior. To initiate the experiment, desired amount of catalyst and H_2O_2 were added. The mixture was mechanically stirred during the reaction. All tests were carried out in ambient conditions at temperature of 20 °C. At predetermined time intervals, 1.0 mL samples were collected and immitted into 1.0 mL of methanol to quench reactive radicals. Then, the samples were immediately filtered through 0.22 μm PES syringe filters to remove solid particles. The concentration of residual BPA was determined by high performance liquid chromatography (HPLC). The results were reproducible within the experimental errors (±5%). At least duplicate runs for each measurement were carried out, and the average values and the standard deviations were presented at the same time. The analysis of BPA degradation kinetics was described by pseudo-first-order model shown in SI Text S2.

To investigate contribution of homogeneous reaction in the MS-Fe Fenton-like system, 0.2 g/L MS-Fe solid was added into 0.2 mM BPA solution with initial pH of 7.0. After being shaken for 30 min, the slurry was immediately filtered to remove the solid. Then the homogeneous catalytic Fenton reaction was initiated by adding predetermined amount of H_2O_2 without adjusting solution pH. The solid was washed with pure water to remove surface impurities, and dried in vacuum oven. To test the role of surface-catalyzed reaction, 0.2 g/L of used solid was added into the solution containing 0.2 mM BPA and 2.0 mM H_2O_2 and the solution pH was preadjusted to be the same as the above filtrate. To evaluate the reusability of the catalyst, the MS-Fe particles were first applied in solutions contained 0.4 mM BPA and 2.0 mM H_2O_2. After the first application, the MS-Fe particles were separated by filtration and dried at 70 °C overnight. Then the reuse performance was evaluated in two different pH conditions: initial pH of 7.0 and 3.1, respectively.

2.5. Analytical procedures

Quantitative analysis of the substances in solution was done using a high performance liquid chromatography (HPLC, LC-20A, Shimadzu, Japan). The HPLC system was equipped with an automatic injector model SIL-20A, LC-20AT pump and a SPD-15C photodiode array detector. A Eclipse XDB-C18 column (5 μm particle size, 4.6 × 150 mm, Agilent, USA) was utilized in the separation of residual BPA concentration. The maximum absorption wavelength (λ_{max}) of BPA detection was set at 280 nm. A mixture of acetonitrile and water at a 40:60 (v/v) ratio was used as the mobile phase with a constant flow rate of 1.0 mL/min. The injective volume of the sample was 20 μL. The concentration of formed *p*-HBA was analyzed on the same HPLC unit at 270 nm using a ZORBAX SB-C18 column (4.6 × 250 mm) and a mixture of 0.65% TFA aqueous solution and acetonitrile (65:35 v/v) as mobile phase.

To analyze the oxidation intermediates of BPA, the samples with byproducts were prior enriched by means of solid-phase extraction (SPE). The SPE cartridges (Oasis HLB, 6 mL, 250 mg) were preconditioned with 5 mL of dichloromethane, 5 mL of methanol and 5 mL of ultrapure water, respectively. The samples were passed with filtration through the cartridges at a flow rate of ~5 mL/min. Subsequently, the analytes were successively eluted using 5 mL of dichloromethane and methanol, respectively. Therefore, both polar and non-polar analytes can be eluted since BPA is insoluble in dichloromethane. Then, the extracted solution was dehydrated by nitrogen blowing, and another 2 mL dichloromethane or methanol was added after the solvent was totally blown away. The GC–MS analysis for BPA intermediates was carried out using a Thermo Scientific TRACE 1300 GC Ultra system equipped with a TG-5MS capillary column (15 m × 0.25 mm × 0.1 μm). The GC injection was operated in splitless mode with a predetermined temperature program. The initial temperature of GC column was set at 40 °C, then increased to 200 °C at a heating rate of 5 °C/min, finally up to 280 °C at a rate of 10 °C/min and held at 280 °C for 5 min. The electron ionization (EI) mass spectra was recorded at 70 eV electron energy in a full-scan mode for qualitative analyses. The detected peaks were identified according to the NIST date library.

Hydrogen peroxide was measured at 405 nm using a UV–vis spectrophotometer after coloration with $TiSO_4$. The amount of ferrous ions was spectrophotometrically determined at wavelength of 510 nm using o-phenanthroline colorimetric method. Total amount of dissolved iron ions was analyzed by adding oxammonium hydrochloride to reduce ferric ions into ferrous ions. Chemical oxygen demand (COD) was determined using microwave digestion method.

3. Results and discussion

3.1. Catalyst characterization

The morphology of the samples was characterized by FESEM and TEM. As shown in Fig. 1a, the S/Fe-oxalate particles are irregular cubic particles of micrometer-scale size without porous structure before calcination. The S/Fe-oxalate after calcination became MS-Fe which generally remained in cubic shapes but exhibited abundant pores and cracks (Fig. 1b). In contrast, the S-Fe composite prepared by precipitation with sodium hydroxide was smaller in size without porous structure (Fig. S1). The high temperature calcination would induce rapid oxalate decomposition into carbon dioxide and water, subsequently leading to cracks inside the sample. Therefore, we concluded that the layered structure and significant porosity of MS-Fe formed during cube cracking. Pores with different size range were generated in MS-Fe where lots of cracks could be easily found on material surface. The existence of mesoporous structure could further be observed by TEM (Fig. 1c). Moreover, the internal structure of MS-Fe composite exhibits particles in nano-size aggregates with mesoporous structures (Fig. 1d).

To test the BET surface area, N_2 adsorption–desorption isotherms were measured and the BJH adsorption pore size distribution plots of MS-Fe, M-Fe and S-Fe composites were obtained as shown in Fig. S2. The pore structure parameters are summarized in Table 1. MS-Fe exhibited a type IV isotherm of IUPAC classification with a H3 hysteresis loop (Fig. S2a) suggesting a multilayered mesoporous structure. The BJH pore size distribution of the MS-Fe composite (inset in Fig. S2a) was focused between 2 nm and 30 nm proving mesoporous structrues. Meanwhile, the S-Fe composite prepared using sodium hydroxide showed a type II isotherm with a H3 hysterresis loop (Fig. S2b), corresponding to monolayer adsorption on nonporous or macroporous material. As shown in Table 1, the BET surface area and pore volume of MS-Fe were calculated to be 151.6 m^2/g and 0.343 cm^3/g, while those of S-Fe were 47.1 and 0.176 cm^3/g, respectively. The MS-Fe composite possessed a much larger surface area and pore volume than nonporous S-Fe composite.

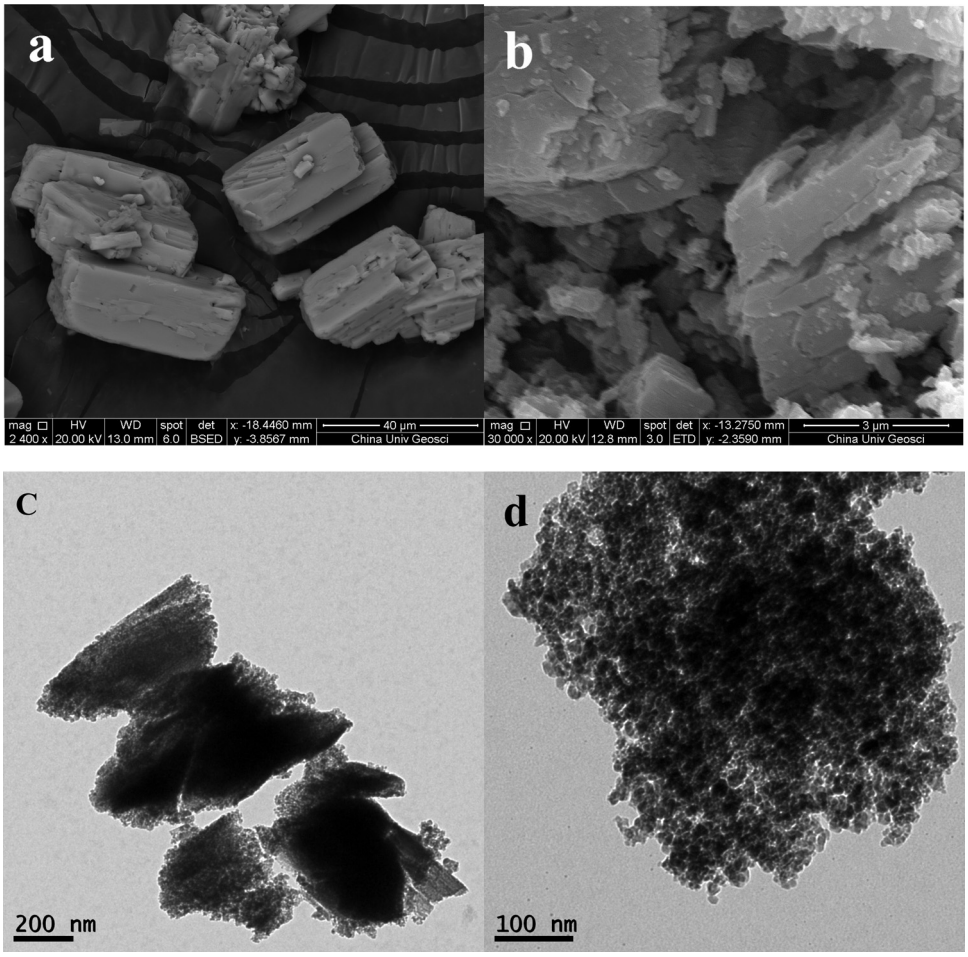

Fig. 1. FESEM image of the MS-Fe particles (a) before and (b) after calcination; (c) and (d) TEM images of the MS-Fe particles after calcination.

Table 1
BET surface area and pore volume parameters for MS-Fe and S-Fe composites.

Sample	BET surface area (m^2/g)	Average pore diameter (nm)	Cumulative pore volume (cm^3/g)
MS-Fe	151.6	6.845	0.343
S-Fe	47.1	19.126	0.176

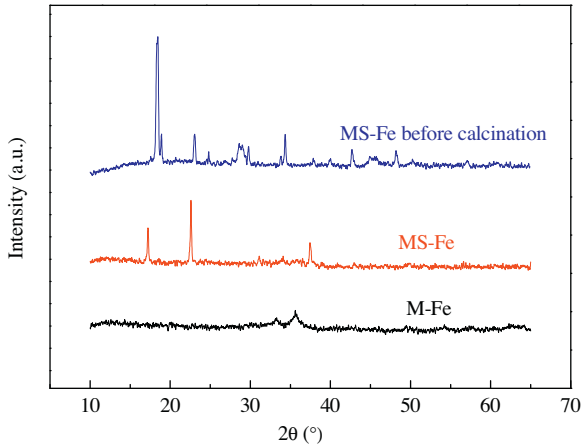

Fig. 2. XRD spectra of M-Fe, MS-Fe before and after calcination.

XRD patterns shown in Fig. 2 were determined to identify the structural properties and investigate the composition variations of the as-prepared materials. The weak and dull diffraction peaks of M-Fe (bottom graph in Fig. 2) indicated low crystallinity of the sample. Two main reflections 2θ at 33.3° and 35.6° were indexed to the facets of hematite Fe_2O_3 (1 0 4) and (1 1 0), respectively [21,23]. For sulfur modified iron oxide, the XRD patter of MS-Fe before calcination matched well with iron oxalate (top graph in Fig. 2). After calcination, the MS-Fe composite (middle graph in Fig. 2) has shown an unidentified XRD pattern with 2θ peaks at 17.2°, 22.6°, 37.5° which may be ascribed to sulfur-doped iron oxide [24].

EDX analyses were conducted to study the surface element distribution and composition in the resultant MS-Fe composite (Fig. S3). The EDX elemental mapping corresponding to the SEM image confirms the presence of sulfur element in MS-Fe which mainly consist of iron, oxygen and sulfur. The composition parameters obtained from EDX profile showed that sulfur had a spot concentration of 5.65% for weight ratio and 5.69% for atomic ratio, respectively.

The FTIR characterization of the M-Fe and MS-Fe composites were conducted to understand the bonding status of sulfur atoms on the oxide surface (Fig. S4). Compared to M-Fe, several new IR bands observed at 1358, 1315, 1194, 1092, 819 cm^{-1} were originated from sulfur containing species [25]. Specifically, the bands centered at 1358 and 1315 cm^{-1} could be attributed to the stretch-

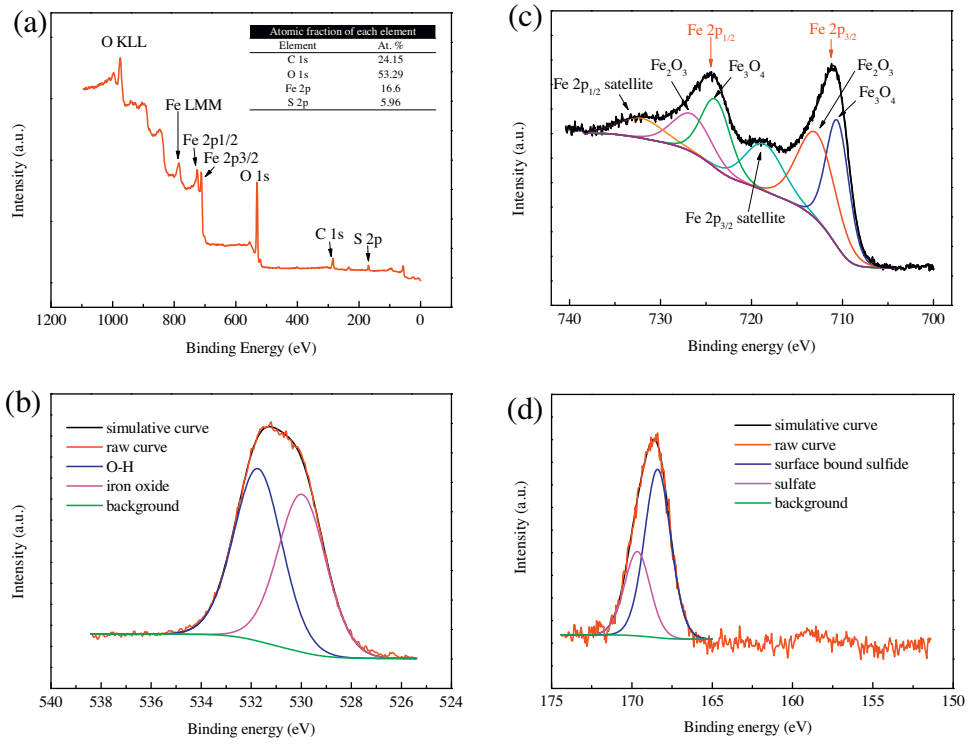

Fig. 3. XPS spectra of as-prepared MS-Fe composite.

ing vibration of S—O group. The bands at 1194 and 1092 cm^{-1} were assigned to surface-bounded SO_3^{2-}/SO_2, which were generated through heat-decomposition of thiosulfate [25], and the peak located at 819 cm^{-1} indicated the presence of sulfite. Additionally, a blue shift of O—H bond from 3405 to 3310 could be due to the electron density transfer to neighboring S—O bond as previously reported [26].

The chemical state of surface elements of MS-Fe composite was further determined by XPS measurements. The survey XPS spectra shows that the MS-Fe composite contains elements of C, O, Fe, S (Fig. 3a). The relative atomic fraction of the four elements (C 1s, O1s, Fe 2p, S 2p) were calculated by peak areas to be 24.15%, 53.29%, 16.6%, 5.96%, respectively. The atomic fractions of O and S were quite coincide to those obtained by EDX, proving the existence of sulfur element. The O 1s spectrum could be fitted to two peaks at 531.73 and 529.97 eV, which can be attributed to O—H group and iron oxide (Fig. 3b). The raw Fe 2p spectra were composed of six fitted curves (Fig. 3c). The binding energies at 710.5 eV and 723.9 eV should be the XPS peaks of Fe $2p_{3/2}$ and Fe $2p_{1/2}$ for Fe_3O_4 [27]. Furthermore, the peaks at 712.8 eV and 726.5 eV associated with a satellite peak obtained at 718.6 eV corresponded to Fe $2p_{3/2}$ and Fe $2p_{1/2}$ for Fe_2O_3. The additional peaks at 732.1 eV might be a satellite peak of Fe $2p_{1/2}$. The S 2p XPS spectrum in Fig. 3d shows two peaks at 168.4 eV and 169.7 eV, corresponding to surface bound sulfite and sulfate, respectively [25,28]. The other small peak at an binding energy of 159.4 eV could be ascribed to iron bonded sulfide (S^{2-}). Therefore, it is reasonable to propose that MS-Fe is a composite material with a mixture of Fe_2O_3, Fe_3O_4 and sulfur-doped iron oxide. As depicted from the characterization of XRD, EDX, FTIR and XPS, the sulfur was mainly existed as sulfite, sulfide and doped sulfur in the oxide matrix.

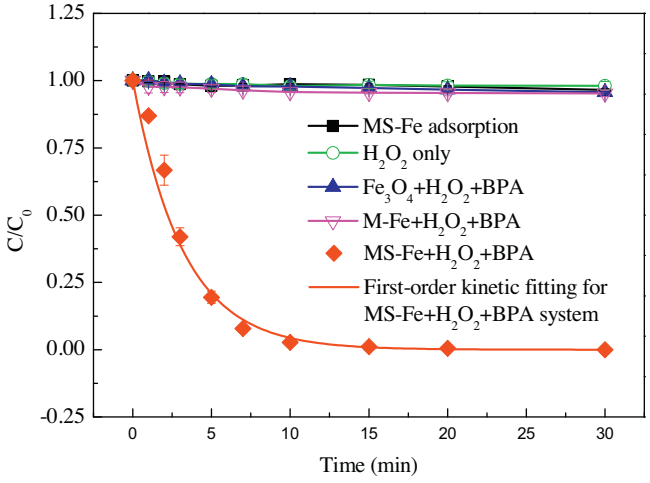

Fig. 4. Degradation of BPA at various reaction processes. Conditions: BPA concentration = 200 μmol/L, initial H_2O_2 concentration = 2.0 mmol/L, catalyst dose = 0.2 g/L, initial pH 7 and ambient temperature.

3.2. Catalytic degradation of BPA

The BPA degradation in aqueous solution was investigated under neutral pH condition by various Fenton-like systems to evaluate their oxidative capacity. As shown in Fig. 4, the complete degradation of 0.2 mM BPA was achieved within 30 min by MS-Fe/H_2O_2 system. The degradation performance could be well fitted by first-order-kinetic model with a correlation coefficient of 0.983. The obtained rate constant of the MS-Fe + H_2O_2 + BPA system was evaluated to be 0.313 min^{-1}. The BPA concentration change was negligible in the absence of either MS-Fe composite or H_2O_2, excluding the effect of volatilization and adsorption. Since BPA

can hardly degraded by H_2O_2 alone, the H_2O_2 should be catalytically decomposed to generate reactive species responsible for BPA degradation. Furthermore, when mesoporous Fe_2O_3 without sulfur doping (M-Fe) was used as Fenton-like catalyst instead of MS-Fe, only 4% BPA abatement was achieved in 30 min reaction. Same situation was observed in Fe_3O_4/H_2O_2 system, implying very weak H_2O_2 activation activity of non-modified iron oxides at neutral pH conditions. The catalytic performance of the MS-Fe composite was further evaluated by decomposing other contaminants with different structural under neutral pH conditions as well as estimating their mineralization degree (Fig. S5). The degradation of rhodamine B, 2,4-dichlorophenol, and BPA was successfully carried out at an initial pH of 7. All the contaminants were completely decomposed within 60 min reaction. The mineralization of the substances was confirmed with significant decrease of COD, which was 58.3% for rhodamine B, 35.05% for 2,4-dichlorophenol, and 54.9% for BPA, respectively.

The solution pH is an important control variable in Fenton or Fenton-like processes since these reactions are usually possible under acidic conditions because of inactivation of iron ions above pH 5. Fig. 5a shows the catalytic performance of MS-Fe composite at different initial pHs. The MS-Fe composite coupled with H_2O_2 was highly effective for BPA degradation at a broad initial pH range of 3.0–9.0, wherein 100% of BPA was removed within 30 min reaction. The degradation profile of BPA followed first-order kinetics at different initial pH values (Fig. S7a). The rate constants were in linear relationship with initial solution pH (Fig. S8a), indicating a pH-dependence degradation behavior. Moreover, the k values at pH 3 and pH 9 were calculated to be 0.406 and 0.300 min^{-1}, being in a narrow range (Table 2). The good efficiency of MS-Fe at different initial pH is a great advantage for its practical application as a Fenton-like catalyst on account of avoiding costly pretreatment of acidification.

Herein, the good performance of MS-Fe at different initial pH should be ascribed to multiple factors including the inherent surface characteristic of MS-Fe composite which may influence the solution pH. We monitored the pH change before and after the reaction for the MS-Fe + H_2O_2 + BPA system (Table 2). The solution pH decreased to 3.4–3.5 when the initial pH value was higher than 3.0, and remained unchanged for initial pH 3 (Table 2). To further investigate the role of MS-Fe composite on solution pH adjusting, 0.5 g/L MS-Fe composite was dispersed into 100 mmol/L KCl solution with different initial pHs in range of 4–11. The solutions were rotary stirred for 24 h to reach equilibrium and the final pH changes were recorded. As shown in Fig. S6, irrespective of the initial pH values, the final pH of all solutions were measured in range of 4.4–5.4. For instance, the solution pH decreased to 5.33 when the initial pH was 11, implying the strong acid–base buffer function of MS-Fe composite. However, no pH change was observed during the same process when non-modified M-Fe oxide was added instead of MS-Fe. Therefore, it is reasonable to propose that the solution pH can be self-controlled to be acidic in the MS-Fe + H_2O_2 + BPA system due to the buffer effect of MS-Fe. Moreover, MS-Fe composite could also self-control the solution pH by producing protons via the Fenton-like reactions between S-modified iron and H_2O_2 [9,12]. For instance, Toda et al. reported the degradation of methylene blue by S-limonite, and the pH of the reacting solution could be self-controlled to around 4 by producing protons via reactions between FeS_2 and H_2O_2, avoiding halfway acid addition [9]. Furthermore, the production of organic acids from BPA decomposition could also contribute to the pH decrease. Since the MS-Fe composite was a strong solid acid in neutral or base conditions, it could create an acidic microenvironment near the surface facilitating the generation of hydroxyl radicals [29]. More than that, this lower pH environment endow •OH with a stronger oxidation capacity, the value of which is about 1.90 V at pH 7.0 but reaches 2.65–2.80 V at pH 3.0 [30].

The effect of initial concentration of H_2O_2 on BPA degradation was also investigated. As shown in Fig. 5b, a faster BPA degradation rate was obtained when increasing H_2O_2 concentration from 1.0 mM (k = 0.156 min^{-1}) to 2.0 mM (k = 0.329 min^{-1}), and the final removal rate of BPA was 92.2% and 100%, respectively. This is probably due to that 1.0 mmol/L H_2O_2 was not enough to completely decompose the given amount of BPA. However, further increasing the H_2O_2 concentration to 4.0 mM did not enhance the degradation rate significantly, and a higher dosage of H_2O_2 (6 mmol/L) led to even slight decrease of BPA decomposition. The k value decreased from 0.47 to 0.45 min^{-1} as the H_2O_2 concentration was increased from 4.0 to 6.0 mmol/L. Same phenomenon has been previously reported in $CuFeO_2$-H_2O_2 system [18], FeOOH-H_2O_2 system [10], etc. The excessive H_2O_2 would react with hydroxyl radical and lead to H_2O_2 consumption, thus causing unwanted scavenging effect as suggested by equations below.

$$H_2O_2 + {}^{\bullet}OH \rightarrow H_2O + {}^{\bullet}O_2H \quad (1)$$

$${}^{\bullet}O_2H + {}^{\bullet}OH \rightarrow H_2O + O_2 \quad (2)$$

Higher catalyst loading can provide more reactive sites for H_2O_2 activation, thus producing more active hydroxyl radicals (Fig. 5c). The oxidation of BPA was accelerated when the catalyst concentration increased from 0.05 g to 0.5 g/L. The degradation rate constant linearly increased with the amount of catalyst loading (Fig. S8c). This observation suggested that H_2O_2 was catalytically decomposed but produced hydroxyl radicals was not scavenged by excessive amount of catalyst, proving a good catalytic performance of the MS-Fe composite. The initial concentration of target contaminant was also an important parameter deduced from the collision theory of chemical reaction. The effect of different initial BPA concentration was shown in Fig. 5d. The removal efficiency of BPA dropped from 100% to 68.5% when the initial BPA concentration increased from 0.1 mM to 0.8 mM. The degradations followed pseudo-first-order kinetics (Fig. S7d), and the k values exhibited a negative linear correlation with initial BPA concentrations, which was coincide with the stoichiometric ratio of generated •OH to the number of BPA molecules (Fig. S8d). The rise of contaminant concentration would poison catalytic sites, retard the interaction between oxidant and catalyst, further decrease the effective collisions between BPA and •OH radicals.

3.3. Identification of reactive radicals

The oxidation of BPA can be induced by reactive radicals (•OH, $^{\bullet}O^{2-}$/$^{\bullet}O_2H$ and ferryl ions), which were produced from catalytic H_2O_2 decomposition [19,31]. •OH is widely regarded as the main active oxidant in most cases. Recently, however, some studies also proposed Fe(IV) as the active species in Fenton process [32]. To distinguish •OH from other radical species, the oxidative transformation of benzoic acid (BA) to its hydroxyl derivative *p*-hydroxybenzoic acid (*p*-HBA) was applied as a probe reaction for •OH measurement [33]. The accumulation of *p*-HBA was proportional to generated •OH, thus quantitatively indicated the formation of OH in aqueous solution. Fig. 6 shows the decomposition rate of H_2O_2 in the MS-Fe/H_2O_2 system and the production of *p*-HBA in the MS-Fe/H_2O_2/BA system. The H_2O_2 decomposed rapidly in the initial stage and became slower with a tailing behavior. Within 30 min reaction, 75% of the added H_2O_2 decomposed over MS-Fe composite at an initial pH of 7. The acidic microenvironment around MS-Fe composite would accelerate H_2O_2 decomposition and facilitate the production of •OH radicals [30]. The H_2O_2 consumption rate correlated well with the

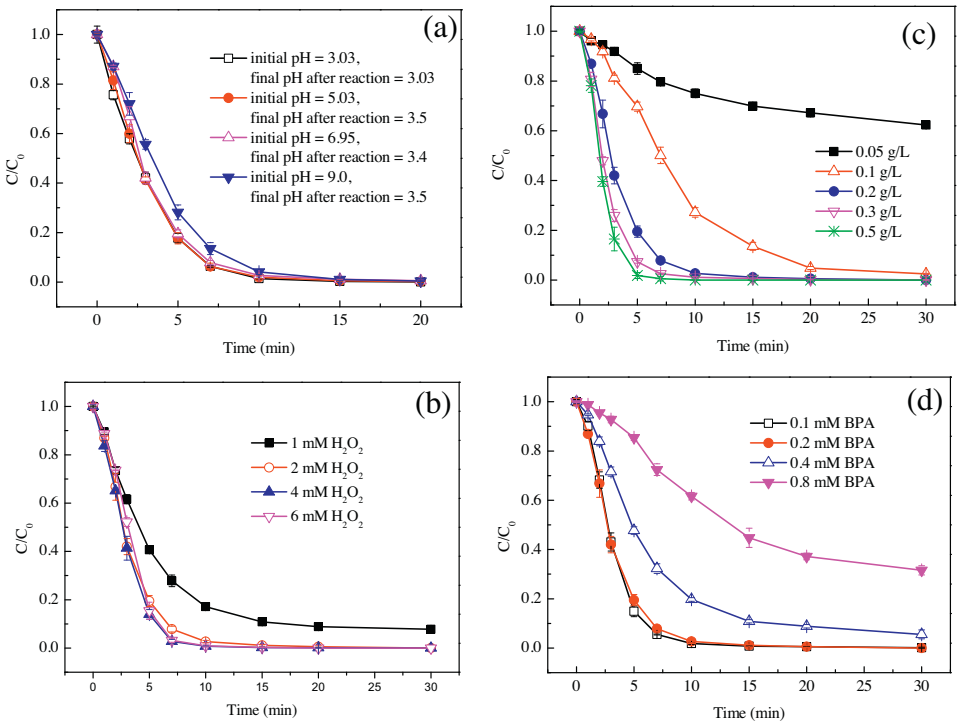

Fig. 5. The effect of various parameters (a) initial pH; (b) H_2O_2 concentration; (c) catalyst dose; (d) BPA concentration on BPA degradation in MS-Fe catalyzed Fenton-like system. Except for the investigated parameter, other parameters fixed at BPA = 200 μmol/L, initial H_2O_2 = 2.0 mmol/L, catalyst dose = 0.2 g/L, initial pH 7 and ambient temperature.

Table 2
Results summarized for BPA degradation.

No.	Variation parameters[a]	pH		Removal rate of BPA[b]	ƙ[c] min^{-1}	R^2 for ƙ
		Initial	Final			
1	pH	3.03	3.03	100%	0.4063	0.995
2	pH	5.03	3.5	100%	0.3725	0.983
3	pH	6.95	3.4	100%	0.329	0.968
4	pH	9.02	3.5	99.8%	0.2996	0.987
5	0 g/L MS-Fe	7.01	7.01	1.92%	–	–
6	0.05 g/L MS-Fe	6.96	5.38	37.7%	0.024	0.956
7	0.10 g/L MS-Fe	7.16	3.59	97.5%	0.146	0.981
8	0.20 g/L MS-Fe	6.95	3.4	100%	0.329	0.968
9	0.30 g/L MS-Fe	6.96	3.53	100%	0.496	0.971
10	0.50 g/L MS-Fe	7.10	3.45	100%	0.869	0.986
11	1.0 mM H_2O_2	7.02	3.39	92.2%	0.156	0.971
12	4.0 mM H_2O_2	6.94	3.33	100%	0.472	0.969
13	6.0 mM H_2O_2	6.99	3.44	100%	0.446	0.951
14	0.1 mM BPA	7.13	3.54	99.9%	0.363	0.952
15	0.4 mM BPA	6.85	3.80	94.5%	0.161	0.988
16	0.8 mM BPA	7.12	3.97	68.4%	0.058	0.989
17	0.2 g/L MS-Fe, no H_2O_2	6.9	4.47	3.5%	–	–
18	0.2 g/L nano-sized Fe_3O_4	6.97	6.96	4.35%	–	–
19	0.2 g/L M-Fe	7.01	6.95	4.76%	–	–

[a] Unless otherwise stated, the reaction conditions are based on 0.2 mM TCE, 2.0 mM H_2O_2, 0.2 mg/L MS-Fe, ambient environment.
[b] The removal rate of BPA in 80 min of degradation time.
[c] ƙ is the pseudo-first-order rate constant.

p-HBA generation rate, and also showed the same trend as that of BPA decay, verifying the predominant contribution of •OH to BPA degradation. To further investigate the role of •OH on BPA oxidation, *t*-butanol and methanol were used as powerful scavengers for •OH (Fig. S9). The addition of quenching alcohols completely suppressed the degradation of BPA, reconfirming that •OH was the primary oxidative species in the MS-Fe/H_2O_2 Fenton-like system.

3.4. Catalyst stability and reaction mechanisms

The reuse performance of the MS-Fe catalyst was evaluated at different pH conditions: initial pH 7.0 and 3.1, respectively. The catalyst reactivity of MS-Fe significantly decreased after the first application (Fig. S10). Specifically, when the catalyst was reused at initial pH of 7.0, only about 7% BPA was removed compared to complete removal in the first run. However, when reused at initial pH of 3.1, 57% and 30% of BPA was removed in the second and third run, respectively. On one hand, the loss of effective sulfur could result

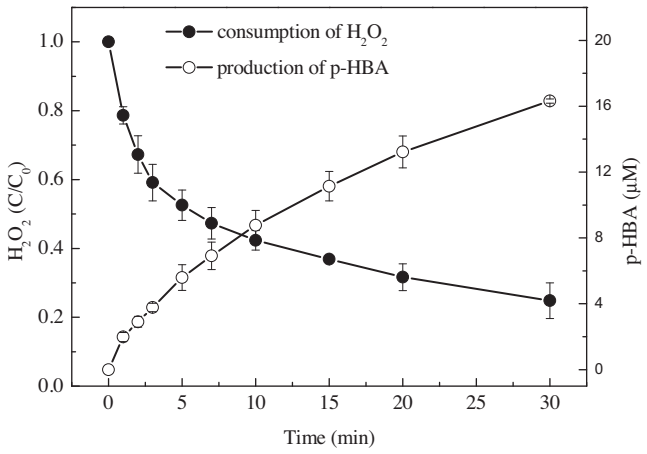

Fig. 6. The time profile of H_2O_2 consumption and *p*-HBA formation during the oxidation of BA in the MS-Fe/H_2O_2 system. Conditions: BA concentration = 5 mmol/L, H_2O_2 concentration = 2.0 mmol/L, catalyst dose = 0.2 g/L, and initial pH 7.

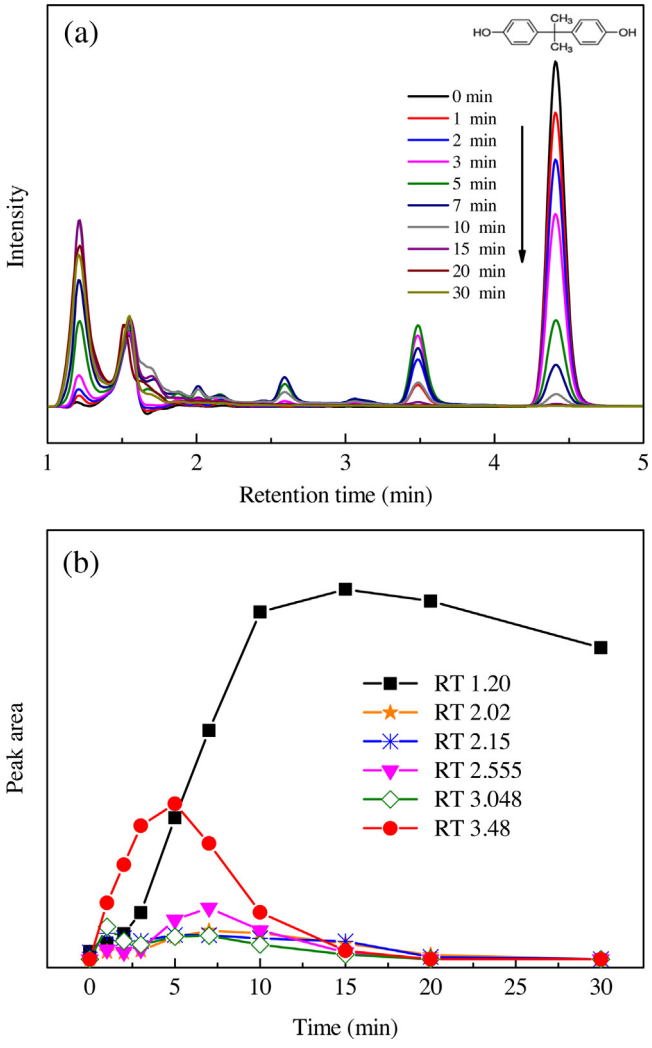

Fig. 7. (a) HPLC diagrams showing the time-dependent formation of byproducts during BPA oxidation in MS-Fe/H_2O_2 system. (b) Time course variation of byproduct concentrations in terms of peak areas. (RT: retention time).

in great decrease of active sites as bare iron oxide showed little Fenton-like catalysis. On the other hand, the MS-Fe composite lost buffer effect after first application, leading to ineffective reusability at initial pH of 7.0 compared to pH of 3.1.

The catalyzed degradation of BPA could take place on catalyst surface and in homogeneous solution. To investigate respective contribution of homogeneous and heterogeneous reactions in MS-Fe/H_2O_2 Fenton-like system, the MS-Fe slurry without H_2O_2 was stirred for 30 min and then filtered to collect the filtrate and solids. The degradation of BPA in the filtrate was processed by adding H_2O_2 without adjusting pH (the filtrate pH was about 4.5). After 30 min of reaction, 83% of BPA was removed in this homogeneous Fenton system (Fig. S11). The solution pH further dropped to 3.5, which could be the result of generated organic acids. The homogeneous Fenton oxidation can proceed via equations below:

$$Fe(II) + H_2O_2 \rightarrow Fe(III) + {}^{\bullet}OH + OH^- \quad (3)$$

$$Fe(III) + H_2O_2 \rightarrow Fe(II) + {}^{\bullet}OH + H^+ \quad (4)$$

The residue of MS-Fe solid was collected, rinsed by ultrapure water, dried in vacuum oven, and then subject to BPA degradation with initial pH of 4.5 which is the pH value of the filtrate. 51% of BPA abatement was achieved after 30 min of reaction and leaching of ferrous ions was negligible in the final solution (Fig. S11). These results indicated a synergistic effect between the homogeneous and heterogeneous degradation. Since the only difference between MS-Fe and M-Fe was the addition of sulfur to MS-Fe, the great improvement of catalyst activity of MS-Fe should be due to sulfur modification. The origin of promoted reactivity could be considered in three aspects. Firstly, the MS-Fe composite possesses strong acidic property after sulfur modification, thus can neutralize considerable amount of hydroxyl group and have a negatively charged surface. More counterbalanced H^+ ions were generated simultaneously. They created an acidic environment, facilitating hydroxyl radical generation. Secondly, as indicated by the O 1s XPS spectrum of used MS-Fe catalyst (Fig. S12a), the OH peak at 531.7 eV significantly intensified compared to fresh MS-Fe, accounting for 80% of all surface O 1s components. These hydroxyl groups cover the MS-Fe surface and serve as a bridge for H_2O_2 and iron species. Then, the highly hydroxylated MS-Fe surface linked with H_2O_2 via electrophilic and hydrogen bonding, forming surface peroxide species, such as Fe(III)—OH—H_2O_2 complex [19]. These surface-bonded peroxide can be easier to decompose via electrophilic attack by intermolecular iron species, thus more reactive hydroxyl radicals could be generated in the acidic environment [18,34,35]. Thirdly, the surface-adsorbed and doped sulfur species drew more electron density from surface-bounded OH group to iron, which can be evidenced by delocalization of O—H bond as depicted in FTIR spectra (Fig. S4). Moreover, the XPS binding energy of surface-bonded OH also left-shifted from 531.73 to 531.34 (Fig. S12a), further indicating the change of electron density. This electron rearrangement could have accelerated decomposition of the surface bonded peroxide and resulted in faster Fe(II)/Fe(III) redox reactions as well, further promoting the production of OH radicals. Meanwhile, by comparing the XPS spectra of S 2p before and after reactions (Fig. S12b), the S 2p peak intensity decreased and the binding energy slightly red-shifted, suggesting that part of attached sulfur species were consumed and oxidized. Similar phenomenon was observed for S-limonite reported by Toda et al. [9]. However, they found that the sulfur peaks of S-limonite was absent in XPS spectra after reacting with H_2O_2 due to the dissolution of sulfate.

3.5. Degradation pathways of BPA decomposition

To understand the degradation pathway of BPA by MS-Fe catalyzed Fenton-like oxidation, the formed intermediates were

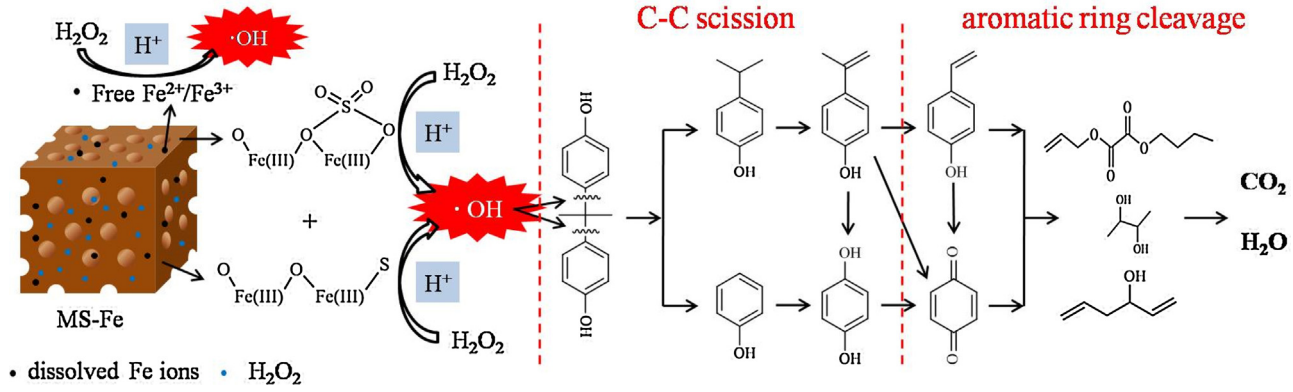

Fig. 8. Proposed degradation pathways for BPA degradation induced by hydroxyl radicals in MS-Fe/H_2O_2 Fenton-like system.

investigated by HPLC as well as GC–MS analysis. The HPLC chromatogram clearly shows the formation of several byproducts which appeared at shorter retention times than BPA, indicating smaller molecular structures and higher polarity of byproducts (Fig. 7a). The time-dependent variation in byproduct contents could be monitored by calculating peak areas, indicating that all BPA byproducts were accumulated at first and further decomposed and degraded (Fig. 7b). All the byproducts almost diminished after 30 min of reaction except one species with the shortest retentions time (RT 1.20), which accumulated while others diminishing. In view of its short retention time at only 1.20 min, the byproduct of RT 1.20 is highly possible to be aliphatic acids.

The oxidative byproducts of BPA were further analyzed by GC–MS, using the NIST date library (byproducts information summarized in Fig. S13 and Table S1). Both aromatic and aliphatic-ring opening products were detected in the present study, including 4-isopropenyl phenol, *p*-benzoquinone, *p*-methoxystyrene, oxalic acid, etc. A primary degradation pathway of BPA was schematically proposed based on our results and previous reports (Fig. 8). The MS-Fe catalyzed Fenton degradation of BPA underwent CC bonds scission on the two middle benzene rings, resulting in formation of phenol and *p*-isopropyl phenol [36,37]. Further attack of •OH radicals induced the dehydration of *p*-isopropyl phenol, which was proved by occurrence of *p*-isopropenyl phenol. Even though hydroquinone was not found in the present GC–MS spectra, it was detected along with *p*-benzoquinone as the major oxidative intermediates in the previous studies [37–39]. Therefore, it was highly possible that phenol was converted into hydroquinone via capturing electrophilic •OH before transformed to *p*-benzoquinone [39]. Additionally, the aromatic molecules would be further oxidized to aliphatic acids. As COD values were observed to decrease significantly (Fig S5), we concluded that the reaction pathways of BPA decomposition went down to the complete mineralization to CO_2 and H_2O.

4. Conclusion

The present work have shown a kind of mesoporous iron oxide modified with sulfur element (MS-Fe), which can be prepared via a simple two-step precipitation–calcination process. This new material exhibited excellent performance in H_2O_2 activation, which efficiently generates •OH radicals for degradation of BPA. The physico-chemical features of MS-Fe and bare M-Fe are understood using characterizations of BET surface area measurement, SEM, XRD, FTIR and XPS. The main conclusions of this study are drawn as follows:

(i) The MS-Fe composite has large BET surface area and appeared as cubic microparticles with abundant pores and cracks. According to results of various characterizations, M-Fe is mainly consisted of hematite while MS-Fe is identified as a kind of S-doped iron oxide with about 5–6% of sulfur element in terms of atomic ratio.

(ii) The MS-Fe composite has shown remarkably high catalytic activity in activating H_2O_2 for BPA degradation in a initial pH range of 3.0–9.0. The MS-Fe composite exhibited an acid–base buffer effect during the reactions because of its strong acidic property. This active catalytic reactivity provides a great advantage over classic Fenton process.

(iii) The time-dependent BPA degradation followed pseudo-first-order kinetics under various reaction parameters. The H_2O_2 dosage has a dual effect on BPA degradation since excessive H_2O_2 addition would lead to scavenging of hydroxyl radicals. Slower degradation rates were observed with increasing initial BPA concentration or decreasing catalyst dosage. Furthermore, the first-order rate constants showed linear relationships with parameters of initial pH, catalyst dosage and BPA concentration, respectively.

(iv) Hydroxyl radicals were the main reactive species responsible for degradation of BPA in the MS-Fe/H_2O_2 system, which displayed a synergistic effect of homogeneous and heterogeneous process. A strong acidic microenvironment due to MS-Fe, abundant surface-bonded hydroxyl groups and electron-mediating effect of sulfur all contributed to fast activation of H_2O_2 and generation of •OH.

(v) Intermediates of BPA, including 4-isopropenyl phenol, *p*-benzoquinone, *p*-methoxystyrene, oxalic acid, were detected via GC–MS analyses. The time-dependent variation of HPLC diagrams showed that these BPA byproducts were accumulated and further decomposed.

Acknowledgements

This study was funded by National Natural Science Foundation of China (41373083) and the National Research Foundation of Korea (NRF) grant funded by the Korea government (MSIP) (No. 2015R1A2A2A04004411). We thank Dr. Songhu Yuan for supporting analytical work.

Appendix A. Supplementary data

Supplementary data associated with this article can be found, in the online version, at http://dx.doi.org/10.1016/j.apcatb.2015.11.015.

Reference:

[1] C.J. Moore, Environ. Res. 108 (2008) 131–139.
[2] R.P. Schwarzenbach, B.I. Escher, K. Fenner, T.B. Hofstetter, C.A. Johnson, U. von Gunten, B. Wehrli, Science 313 (2006) 1072–1077.
[3] J. Annamalai, V. Namasivayam, Environ. Int. 76 (2015) 78–97.
[4] B.R. Petigara, N.V. Blough, A.C. Mignerey, Environ. Sci. Technol. 36 (2002) 639–645.
[5] A.D. Bokare, W. Choi, J. Hazard. Mater. 275 (2014) 121–135.
[6] S. Yuan, X. Mao, A.N. Alshawabkeh, Environ. Sci. Technol. 46 (2012) 3398–3405.
[7] S. Rahim Pouran, A.A. Abdul Raman, W.M.A. Wan Daud, J. Cleaner Prod. 64 (2014) 24–35.
[8] Y. Wang, H. Zhao, G. Zhao, Appl. Catal. B 164 (2015) 396–406.
[9] K. Toda, T. Tanaka, Y. Tsuda, M. Ban, E.P. Koveke, M. Koinuma, S. Ohira, J. Hazard. Mater. 278 (2014) 426–432.
[10] I.S.X. Pinto, P.H.V.V. Pacheco, J.V. Coelho, E. Lorençon, J.D. Ardisson, J.D. Fabris, P.P. de Souza, K.W.H. Krambrock, L.C.A. Oliveira, M.C. Pereira, Appl. Catal. B 119–120 (2012) 175–182.
[11] I. Velo-Gala, J.J. López-Peñalver, M. Sánchez-Polo, J. Rivera-Utrilla, Chem. Eng. J. 241 (2014) 504–512.
[12] S. Bae, D. Kim, W. Lee, Appl. Catal. B 134–135 (2013) 93–102.
[13] K. Rusevova, F.-D. Kopinke, A. Georgi, J. Hazard. Mater. 241–242 (2012) 433–440.
[14] T.L.P. Dantas, V.P. Mendonça, H.J. José, A.E. Rodrigues, R.F.P.M. Moreira, Chem. Eng. J. 118 (2006) 77–82.
[15] I. Ursachi, A. Stancu, A. Vasile, J. Colloid Interface Sci. 377 (2012) 184–190.
[16] J.V. Coelho, M.S. Guedes, R.G. Prado, J. Tronto, J.D. Ardisson, M.C. Pereira, L.C.A. Oliveira, Appl. Catal. B 144 (2014) 792–799.
[17] Z. Shu, Y. Chen, W. Huang, X. Cui, L. Zhang, H. Chen, G. Zhang, X. Fan, Y. Wang, G. Tao, D. He, J. Shi, Appl. Catal. B 140–141 (2013) 42–50.
[18] X. Zhang, Y. Ding, H. Tang, X. Han, L. Zhu, N. Wang, Chem. Eng. J. 236 (2014) 251–262.
[19] M. Wang, N. Wang, H. Tang, M. Cao, Y. She, L. Zhu, Catal. Sci. Technol. 2 (2012) 187–194.
[20] E.J. Kim, J.H. Kim, A.M. Azad, Y.S. Chang, ACS Appl. Mater. Interfaces 3 (2011) 1457–1462.
[21] L. Guo, F. Chen, X. Fan, W. Cai, J. Zhang, Appl. Catal. B 96 (2010) 162–168.
[22] M. Pu, Y. Ma, J. Wan, Y. Wang, M. Huang, Y. Chen, J. Colloid Interface Sci. 418 (2014) 330–337.
[23] X. Zhang, Y. Niu, Y. Li, X. Hou, Y. Wang, R. Bai, J. Zhao, Mater. Lett. 99 (2013) 111–114.
[24] G. Xie, P. Xi, H. Liu, F. Chen, L. Huang, Y. Shi, F. Hou, Z. Zeng, C. Shao, J. Wang, J. Mater. Chem. 22 (2012) 1033–1039.
[25] L. Zhao, X. Li, C. Hao, C.L. Raston, Appl. Catal. B 117–118 (2012) 339–345.
[26] T. Zhang, H. Zhu, J.P. Croue, Environ. Sci. Technol. 47 (2013) 2784–2791.
[27] T. Yamashita, P. Hayes, Appl. Surf. Sci. 254 (2008) 2441–2449.
[28] G.K. Pradhan, N. Sahu, K.M. Parida, RSC Adv. 3 (2013) 7912–7920.
[29] S. Tian, J. Zhang, J. Chen, L. Kong, J. Lu, F. Ding, Y. Xiong, Ind. Eng. Chem. Res. 52 (2013) 13333–13341.
[30] A.A. Burbano, D.D. Dionysiou, M.T. Suidan, T.L. Richardson, Water res. 39 (2005) 107–118.
[31] S.-Y. Pang, J. Jiang, J. Ma, Environ. Sci. Technol. 45 (2011) 307–312.
[32] H. Lee, H.J. Lee, D.L. Sedlak, C. Lee, Chemosphere 92 (2013) 652–658.
[33] A.D. Bokare, W. Choi, Environ. Sci. Technol. 45 (2011) 9332–9338.
[34] L. Yu, C. Wang, X. Ren, H. Sun, Chem. Eng. J. 252 (2014) 346–354.
[35] S.-S. Lin, M.D. Gurol, Environ. Sci. Technol. 32 (1998) 1417–1423.
[36] T. Olmez-Hanci, I. Arslan-Alaton, B. Genc, J. Hazard. Mater. 263 (2013) 283–290.
[37] V. Cleveland, J.-P. Bingham, E. Kan, Sep. Purif. Technol. 133 (2014) 388–395.
[38] S. Yuan, N. Gou, A.N. Alshawabkeh, A.Z. Gu, Chemosphere 93 (2013) 2796–2804.
[39] J. Poerschmann, U. Trommler, T. Górecki, Chemosphere 79 (2010) 975–986.